INTERNATIONAL JOURNAL FOR NUMERICAL METHODS IN ENGINEERING
Int. J. Numer. Meth. Engng 2005; **62**:1857–1872
Published online 2 February 2005 in Wiley InterScience (www.interscience.wiley.com). DOI: 10.1002/nme.1256

Continuum–discontinuum modelling of shear bands

Esteban Samaniego[‡,§] and Ted Belytschko[*,†]

Department of Mechanical Engineering, Northwestern University, 2145 Sheridan Road, Room A212, Evanston, IL 60208-3111, U.S.A.

SUMMARY

A methodology to model shear bands as strong discontinuities within a continuum mechanics context is presented. The loss of hyperbolicity of the IBVP is used as the criterion for switching from a classical continuum description of the constitutive behaviour to a traction–separation model acting at the discontinuity surface. The extended finite element method (XFEM) is employed for the spatial discretization of the governing equations. This enables the shear bands to be arbitrarily positioned within the mesh. Examples that study the shear band progression within a rate-independent material are presented. Copyright © 2005 John Wiley & Sons, Ltd.

KEY WORDS: finite element method; shear bands; loss of hyperbolicity; traction–separation laws; extended finite element method

1. INTRODUCTION

A shear band can be described as a narrow region in a solid undergoing intense shearing. After a shear band is fully developed, relative sliding of the two sides of the band similar to mode II fracture can be observed. Shear bands can be regarded as specific instances of the more general phenomenon of strain localization and as material instabilities.

When dealing with rate independent materials undergoing strain softening, the development of bands of localized deformation has classically been linked to the loss of hyperbolicity of the linearized initial boundary value problem (IBVP). In Reference [1], a closed form solution was obtained for a wave propagation problem in a one-dimensional bar. It was shown that, despite the loss of positivity of the tangent modulus, a solution could be obtained if the region

*Correspondence to: T. Belytschko, Department of Mechanical Engineering, Northwestern University, 2145 Sheridan Road, Room A212, Evanston, IL 60208-3111, U.S.A.
† E-mail: t-belytschko@northwestern.edu
‡ Post Doctoral Research Fellow, Northwestern University.
§ E-mail: E-msamaniego@northwestern.edu

Contract/grant sponsor: Office of Naval Research

Received 3 September 2004
Revised 6 October 2004
Accepted 18 October 2004

Copyright © 2005 John Wiley & Sons, Ltd.

undergoing strain softening was restricted to a set of (Lebesgue) measure zero. However, the solution was considered to be meaningless from a physical point of view, because it implied zero dissipation. As pointed out by Armero [2], for example, this shows the necessity of including some dissipative mechanism in the region in which hyperbolicity has been lost.

The above discussion highlights two crucial phases of the mathematical modelling of strain localization:

(1) The detection of loss of material stability.
(2) The adoption of some model to capture the post-localization behaviour.

The former determines the material points that belong to a localization band, whereas the latter enables one to obtain physically meaningful solutions after the onset of localization.

In this paper, we adopt the use of interface laws for modelling the post-failure behaviour of the material. Thus, a shear band is regarded as having zero width, and, therefore, as a discontinuity in the displacement field. In light of this, the use of the extended element method (X-FEM) for the spatial discretization of the IBVP emerges as natural because of its ability to include discontinuities in the approximating fields.

The numerical modelling of shear bands by means of some enrichment of the standard finite element method can be traced back to References [3, 4]. The methods proposed in these references belong to the class of the so-called finite elements with embedded discontinuities. Later, the link between the continuum theory of strain localization, the concept of cohesive surfaces, and the use of embedded elements was studied by means of the so-called strong discontinuity analysis in Reference [5]. Further developments of this approach can be found in References [6, 7].

The remainder of this paper is organized as follows. First, the use of the local hyperbolicity of the momentum equation as a criterion of material stability is motivated. Then, the problem of a solid with a dissipative interface is stated. The constitutive equations for the bulk material and the dissipative interface are also discussed. The discretization of the IVBP is then addressed. Later, a means to propagate the shear band tip based on the hyperbolicity indicator is explained. Some examples are used to illustrate the capabilities of the method. Finally, some concluding remarks are given.

2. SHEAR BAND ONSET

As mentioned in the introduction, a shear band in a rate-independent material results from a material instability. The characterization of material instabilities is somehow controversial. A classical definition of material stability is based on the so-called Legendre–Hadamard condition, which establishes that for any non-zero vectors $\mathbf{n}$ and $\mathbf{h}$, the following point-wise inequality must hold:

$$(\mathbf{n} \otimes \mathbf{h}) : \mathbf{A} : (\mathbf{n} \otimes \mathbf{h}) > 0 \tag{1}$$

where $\mathbf{A}$ is the constitutive tangent operator, $\mathbf{n}$ defines the direction of propagation, and $\mathbf{h}$ is the *polarization* of the wave. This condition ensures that the velocity of propagating waves in a solid remains real. Equality in expression (1) is the necessary condition for stationary waves. Reference [8] gives a textbook description for obtaining condition (1) by

Copyright © 2005 John Wiley & Sons, Ltd.

means of a stability analysis of the momentum equation when a perturbation of the form $\boldsymbol{u} = \boldsymbol{h}\exp(\mathrm{i}\omega t + k\boldsymbol{n}\cdot\boldsymbol{x})$ is applied. The Legendre–Hadamard condition is some times called strong ellipticity of the constitutive relation (see Reference [9]). For the quasi-static case, and under certain regularity assumption, this condition is equivalent to rank-one convexity of the underlying potential (see Reference [10]). In the dynamical case, the Legendre–Hadamard condition implies the hyperbolicity of the IBVP. The reader is referred to Reference [11] for further details about the concepts presented above and their interrelation.

Based on expression (1), let us define, for a given material point of a solid at a given time,

$$e := \min_{\boldsymbol{n},\boldsymbol{h}}[(\mathbf{n}\otimes\mathbf{h}) : \mathbf{A} : (\mathbf{n}\otimes\mathbf{h})] \tag{2}$$

where e will be called the hyperbolicity indicator as in Reference [12]. We say that a material point is stable whenever the hyperbolicity indicator e is strictly positive.

2.1. Expression of e for associated plasticity

Let us state the following general expression for the constitutive tangent operator for associated plasticity in small strains:

$$\mathbf{A} = \mathbf{C} - \frac{(\mathbf{C} : \mathbf{m}) \otimes (\mathbf{m} : \mathbf{C})}{H + \mathbf{m} : \mathbf{C} : \mathbf{m}} \tag{3}$$

where H is the hardening/softening modulus, $\mathbf{m}$ is the plastic flow tensor, and $\mathbf{C}$ stands for the isotropic elasticity tensor defined as

$$\mathbf{C} := \lambda\mathbf{1}\otimes\mathbf{1} + 2\mu\mathbf{I} \tag{4}$$

with λ and μ being the Lamè parameters; $\mathbf{1}$ and $\mathbf{I}$ are the second order and the (symmetric) fourth order unit tensors, respectively.

Inserting (3) in (2), we obtain

$$e = \min_{\boldsymbol{n},\boldsymbol{h}}\left[(\lambda+\mu)(\mathbf{h}\cdot\mathbf{n})^2 + \mu\|\mathbf{h}\|^2 - \frac{\lambda(\mathbf{h}\cdot\mathbf{n})Tr(\mathbf{m}) + 2\mu\mathbf{h}\cdot\mathbf{m}\cdot\mathbf{n}}{H + \lambda Tr^2(\mathbf{m}) + 2\mu\|\mathbf{h}\|^2}\right] \tag{5}$$

3. POST-LOCALIZATION BEHAVIOUR

Once the material loses stability, the use of standard governing equations leads to ill-posedness of the IBVP. Nevertheless, as pointed out in Reference [1], a solution can be obtained for wave propagation in a one-dimensional softening bar whenever the unstable region is restricted to a set of measure zero. The lack of physical meaning of the solution obtained (total dissipation equal to zero) can be attributed to the fact that no dissipative mechanism capable of acting in a set of (Lebesgue) measure zero was considered.

Within the context of non-linear fracture mechanics, these dissipative mechanisms have been introduced by means of the so-called cohesive surfaces [13, 14]. We adopt a similar methodology here for modelling shear bands.

Copyright © 2005 John Wiley & Sons, Ltd.

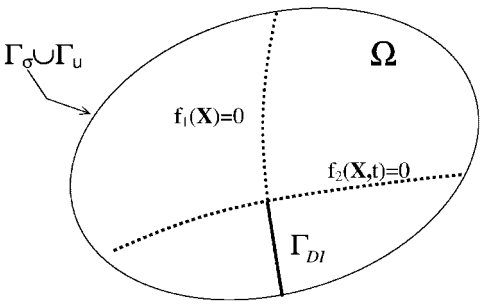


Figure 1. Solid with a dissipative interface.

3.1. IBVP with an internal dissipative interface

Consider a solid Ω with material points $\mathbf{X}$. Its boundary Γ is partitioned into two subsets, Γ_σ and Γ_u, upon which tractions and displacements are prescribed, respectively. The locus of an internal dissipative interface Γ_{DI} is a subset of the zero level set of an implicit function f_1, i.e. the set of all $\mathbf{X} \in \Omega$ such that $f_1(\mathbf{X}) = 0$. This dissipative interface will be used to identify material points for which the hyperbolicity of the governing equations has been lost, i.e. where the hyperbolicity indicator defined in (2) has lost positivity. The unit normal $\mathbf{n}$ to Γ_{DI} can be readily computed as

$$\mathbf{n} = \frac{\nabla f_1}{\|\nabla f_1\|} \tag{6}$$

To specify the edge of the dissipative interface at time t, we construct another implicit function $f_2(\mathbf{X}, t)$ (see Figure 1), as in References [15, 16], whose level sets are orthogonal to those of $f_1(\mathbf{X})$ and such that

$$\Gamma_{\mathrm{DI}} := \{\mathbf{X} \in \Omega;\ f_1(\mathbf{X}) = 0 \text{ and } f_2(\mathbf{X}, t) \geqslant 0\} \tag{7}$$

The position of the tip of a shear band at time t, denoted by $\mathbf{x}^{\mathrm{tip}}(t)$, is given by $f_1(\mathbf{X}) = f_2(\mathbf{X}, t) = 0$.

In the quasi-static case, the solution of a boundary value problem (BVP) with internal boundaries is to be sought, for small strains, in the so-called *Space of Functions with Bounded Deformation* (BD) (see Reference [17]). This space contains functions whose symmetric distributional gradients are bounded (Radon) measures. Within this functional framework, discontinuities in the displacement field can be properly treated. For the dynamical case, it seems reasonable to assume that the restriction of the solution to a given instant of time also belongs to BD.

Based on these considerations, we adopt, as in Reference [18], for a given time t, the following additive decomposition of the displacement field, $\mathbf{u}_t \equiv \mathbf{u}(\cdot, t) : \Omega \to \mathbb{R}^n$, into smooth, $\hat{\mathbf{u}}_t$, and non-smooth part, $\mathbf{u}'_t$:

$$\mathbf{u}_t = \hat{\mathbf{u}}_t + \mathbf{u}'_t \tag{8}$$

where $\hat{\mathbf{u}}_t \in \mathsf{H}^1(\Omega; \mathbb{R}^n)$ and $\mathbf{u}'_t$ is required to fulfil the following conditions:

- $\mathbf{u}'_t = \mathbf{0}$ outside some set $\Omega_{\mathbf{u}'_t} \subset \{\mathbf{X} \in \Omega;\ f_2(\mathbf{X}, t) \geqslant 0\}$ containing Γ_{DI}.

Copyright © 2005 John Wiley & Sons, Ltd.

- For every open set $\mathrm{U} \subset \Omega$ such that $\mathrm{U} \cap \Gamma_{\mathrm{DI}} = \emptyset$, $\mathbf{u}'_t|_{\mathrm{U}}$ is smooth.
- $[\![\mathbf{u}'_t]\!]_{\Gamma_{\mathrm{DI}}} = [\![\mathbf{u}_t]\!]_{\Gamma_{\mathrm{DI}}}$ on Γ_{DI}.

where $[\![\mathbf{u}_t]\!]_{\Gamma_{\mathrm{DI}}}$ denotes the jump of $\mathbf{u}_t$ across the discontinuity interface Γ_{DI}.

We denote the space of functions with elements $\mathbf{u}_t$ satisfying the Dirichlet boundary conditions on Γ_u by S_t. Let us also define the corresponding space of test functions as

$$V := \{\delta\mathbf{u};\ \mathbf{u}_t + \delta\mathbf{u} \in S_t,\ \mathbf{u}_t \in S_t\} \tag{9}$$

Now, we state the following weak form of an IBVP for a solid with an internal dissipative interface Γ_{DI}:

GIVEN the initial displacement, $\mathbf{u}_0$, and the initial velocity, $\dot{\mathbf{u}}_0$,
FIND $\mathbf{u}_t \in S_t$ for every time t in the time interval of analysis
SUCH THAT, for all $\delta\mathbf{u} \in V$,

$$\int_\Omega \rho\delta\mathbf{u}\cdot\ddot{\mathbf{u}}\,\mathrm{d}\Omega = \int_{\Omega\setminus\Gamma_{\mathrm{DI}}} (\nabla \odot \delta\mathbf{u}) : \boldsymbol{\sigma}\,\mathrm{d}\Omega - \int_\Omega \delta\mathbf{u}\cdot\mathbf{b}\,\mathrm{d}\Omega - \int_{\Gamma_\sigma} \delta\mathbf{u}\cdot\mathbf{t}\,\mathrm{d}\Gamma + \int_{\Gamma_{\mathrm{DI}}} \delta[\![\mathbf{u}]\!]\cdot\mathbf{t}_{\mathrm{DI}}\,\mathrm{d}\Gamma \tag{10}$$

in the time interval of analysis. In the above, the symbol $\odot$ denotes the symmetrized tensor product and ρ is the density.

3.2. Constitutive model

We assume that the constitutive behaviour in $\Omega\setminus\Gamma_{\mathrm{DI}}$ is governed by a continuum constitutive model, whereas the material description on Γ_{DI} will be ruled by a traction–separation model (often called a cohesive law). Similar approaches to the modelling of shear bands can be found in References [19, 20].

As to the continuum model, a standard associative plasticity model for small strains with an isotropic hardening/softening law is considered. The state equation for the stress reads

$$\boldsymbol{\sigma} = \mathbf{C} : (\boldsymbol{\varepsilon} - \boldsymbol{\varepsilon}^{\mathrm{p}}) \tag{11}$$

where $\boldsymbol{\varepsilon}^{\mathrm{p}}$ is the plastic strain tensor. The stress-like internal variable is assumed to be a function of the equivalent plastic strain, so

$$g = \mathrm{g}(\varepsilon^*) \tag{12}$$

g denotes the stress-like internal variable and ε^* the equivalent plastic strain. We also have an evolution equation for the plastic strain,

$$\dot{\boldsymbol{\varepsilon}}^{\mathrm{p}} = \gamma \frac{\partial F}{\partial \boldsymbol{\sigma}} = \gamma\mathbf{m} \tag{13}$$

where F is the yield function (which defines the elastic region in the generalized stress space) and γ is the so-called plastic multiplier, as well as an evolution equation for the equivalent plastic strain,

$$\dot{\varepsilon}^* = \gamma \frac{\partial F}{\partial g} \tag{14}$$

Copyright © 2005 John Wiley & Sons, Ltd.

The yield function is defined by

$$F(\boldsymbol{\sigma}, g) = \bar{\sigma}(\boldsymbol{\sigma}) - g \tag{15}$$

where $\bar{\sigma}$ is some scalar valued function of the stress state σ. Function (15) defines the set of admissible states as those for which

$$F(\boldsymbol{\sigma}, g) \leqslant 0 \tag{16}$$

Finally, we have the loading/unloading conditions,

$$\gamma \geqslant 0;\ F(\boldsymbol{\sigma}, g) \leqslant 0;\ \gamma F(\boldsymbol{\sigma}, g) = 0 \tag{17}$$

and the plastic consistency condition,

$$\gamma \dot{F}(\boldsymbol{\sigma}, g) = 0 \tag{18}$$

3.2.1. Interface model. Let us define $\Omega \supset \Omega_i^\eta := \Gamma_i \times (-\eta/2, \eta/2)$, where $\Gamma_i \subset \Gamma_{\mathrm{DI}}$ and η is a positive real number that can be interpreted as the width of the shear band. Then, we assume that there exists a scalar valued function $\dot{\alpha}$ on Γ_{DI}, such that, for any $\Gamma_i \subset \Gamma_{\mathrm{DI}}$, the following equality holds:

$$\int_{\Gamma_i} \dot{\alpha}\mathbf{m}\, \mathrm{d}\Gamma = \lim_{\eta \to 0^+} \int_{\Omega_i^\eta} \underbrace{\gamma \mathbf{m}}_{\dot{\boldsymbol{\varepsilon}}^{\mathrm{p}}}\, \mathrm{d}\Omega \tag{19}$$

We also assume that the elastic strain rate, $\dot{\boldsymbol{\varepsilon}}^{\mathrm{e}} = \dot{\boldsymbol{\varepsilon}} - \dot{\boldsymbol{\varepsilon}}^{\mathrm{p}}$ fulfils

$$\lim_{\eta \to 0^+} \int_{\Omega_i^\eta} \dot{\boldsymbol{\varepsilon}}^{\mathrm{e}}\, \mathrm{d}\Omega = \mathbf{0} \tag{20}$$

The above assumptions are motivated by the high plastic strains that occur in a shear band. The main contribution to the highly localized strains comes from the plastic part. Thus the elastic strains are negligible.

Considering Equation (8), it can be shown that, for any $\Gamma_i \subset \Gamma_{\mathrm{DI}}$,

$$\lim_{\eta \to 0^+} \int_{\Omega_i^\eta} \dot{\boldsymbol{\varepsilon}}\, \mathrm{d}\Omega = \int_{\Gamma_i} (\llbracket \dot{\mathbf{u}} \rrbracket \odot \mathbf{n})\, \mathrm{d}\Gamma \tag{21}$$

From Equations (19)–(21) we obtain

$$\int_{\Gamma_i} \dot{\alpha}\mathbf{m}\, \mathrm{d}\Gamma = \int_{\Gamma_i} (\llbracket \dot{\mathbf{u}} \rrbracket \odot \mathbf{n})\, \mathrm{d}\Gamma \tag{22}$$

for any $\Gamma_i \subset \Gamma_{\mathrm{DI}}$. Hence,

$$\dot{\alpha}\mathbf{m} = \llbracket \dot{\mathbf{u}} \rrbracket \odot \mathbf{n} \quad \text{on } \Gamma_{\mathrm{DI}} \tag{23}$$

Equation (23) was obtained in Reference [21] within the context of the so-called strong discontinuity analysis. It provides us with the means to construct the interface model from the

Copyright © 2005 John Wiley & Sons, Ltd.

continuum constitutive model. Consider, for example, the standard J2 flow plasticity model in small strains, for which

$$\mathbf{m} = \frac{\mathrm{dev}(\boldsymbol{\sigma})}{\|\mathrm{dev}(\boldsymbol{\sigma})\|} \tag{24}$$

where $\mathrm{dev}(\cdot)$ denotes the deviatoric part of $(\cdot)$. Then, the trace of both sides of Equation (23) must fulfil

$$\mathrm{tr}(\dot{\alpha}\mathbf{m}) = [\![\dot{\mathbf{u}}]\!] \cdot \mathbf{n} = 0 \quad \text{on } \Gamma_{\mathrm{DI}} \tag{25}$$

$\mathrm{tr}(\cdot)$ denotes the trace of $(\cdot)$. The above condition implies that, for J2 flow theory, only the jumps in the velocity component tangential to Γ_{DI} are possible.

From Equation (24), we have that $\|\mathbf{m}\| = 1$. Then Equation (23) implies

$$\dot{\alpha} = \|[\![\dot{\mathbf{u}}]\!] \odot \mathbf{n}\| \quad \text{on } \Gamma_{\mathrm{DI}} \tag{26}$$

Consider the two-dimensional case. Let $\mathbf{e}_T$ denote a vector field on Γ_{DI} orthogonal to $\mathbf{n}$. Then, defining $m_{nT} \equiv \mathbf{n} \cdot \mathbf{m} \cdot \mathbf{e}_T$ and $[\![\dot{u}]\!]_T \equiv [\![\dot{\mathbf{u}}]\!] \cdot \mathbf{e}_T$, and considering Equation (23),

$$m_{nT} = \frac{1}{2\dot{\alpha}} [\![\dot{u}]\!]_T \quad \text{on } \Gamma_{\mathrm{DI}} \tag{27}$$

If we define $t_T \equiv \mathbf{n} \cdot \boldsymbol{\sigma} \cdot \mathbf{e}_T = \mathbf{n} \cdot \mathrm{dev}(\boldsymbol{\sigma}) \cdot \mathbf{e}_T = \mathbf{t} \cdot \mathbf{e}_T$, then, from Equation (24),

$$m_{nT} = \frac{t_T}{\|\mathrm{dev}(\boldsymbol{\sigma})\|} \tag{28}$$

Let us consider now Equations (15) and (17), and also that for J2 flow theory $\bar{\sigma}(\boldsymbol{\sigma}) = \|\mathrm{dev}(\boldsymbol{\sigma})\|$. Then, for plastic loading, we have

$$\|\mathrm{dev}(\boldsymbol{\sigma})\| = g \tag{29}$$

Thus, from Equations (27)–(29), we obtain

$$t_T = \frac{g}{2\dot{\alpha}} [\![\dot{u}]\!]_T \quad \text{on } \Gamma_{\mathrm{DI}} \tag{30}$$

In order to have an interface constitutive model driven by the velocity jump, g must be expressed in terms of $[\![\dot{u}]\!]_T$. The natural choice is to establish this relationship through α. In light of this, we propose the following functional relation between g and α:

$$g = \mathrm{g}\left(\varepsilon^*_{\mathrm{SB}}\right) + \tilde{\mathbf{g}}(\alpha) \quad \text{on } \Gamma_{\mathrm{DI}} \tag{31}$$

where $\varepsilon^*_{\mathrm{SB}}$ is the value of the equivalent plastic strain at the time of loss of hyperbolicity. We impose that $\tilde{\mathbf{g}}(\alpha) = 0$ for $\alpha = 0$. Thus, $\mathrm{g}\left(\varepsilon^*_{\mathrm{SB}}\right)$ is the initial value for the softening law acting at the discontinuity interface Γ_{DI}.

4. DISCRETIZATION OF THE IBVP

4.1. Discretization via X-FEM

It is clear that standard finite element formulations are not well suited for the solution of IBVP's as the one posed in (10). Due to the 'roughness' of the BD in which the solution of

Copyright © 2005 John Wiley & Sons, Ltd.

problems with dissipative interfaces lies, standard finite element approximation functions are not able to provide a sharp resolution of the approximated fields. However, the structure of the displacement field given in Equation (8) can be exploited if its smooth part is approximated by standard finite element functions while its non-smooth part is approximated by means of some enrichment. This concept was used in References [22–24] for the study of discontinuities within the context of linear fracture mechanics. Extensions to the study of solids with cohesive surfaces can be found in References [25–27].

In this framework the approximation of the displacement field is

$$\mathbf{u}^h(\mathbf{X},t) = \sum_{I=1}^{n_{\text{nod}}} N_I(\mathbf{X})\mathbf{a}_I(t) + \sum_{I\in\mathbb{J}} \phi_I(\mathbf{X}) q_I(t)\mathbf{e}_T(\mathbf{X}) \tag{32}$$

where n_{nod} is the number of nodes, N_I is a (standard) finite element shape function associated to node I, $\mathbb{J}$ is the set of indices corresponding to the enriched nodes, $\mathbf{a}_I$ are the standard displacement degrees of freedom, $\mathbf{e}_T(\mathbf{X})$ is the unit tangent to the shear band at $\mathbf{X}$, q_I are the displacement degrees of freedom associated with the enrichment, and ϕ_I are enrichment functions defined as

$$\phi_I(\mathbf{X}) = N_I(\mathbf{X})[\mathscr{H}(f(\mathbf{X})) - \mathscr{H}(f(\mathbf{X}_I))] \tag{33}$$

where $\mathscr{H}$ is the Heaviside step function and $\mathbf{X}_I$ is the position vector of node I. Since $\mathbf{e}_T$ is orthogonal to $\mathbf{n}$ and $\mathbf{n}$ is defined by Equation (6), we can see that $\mathbf{e}_T$ is defined by the level set. Note that the enrichment term in Equation (32) acts only in the direction tangential to the shear band, as required by condition (25). By construction, the enrichment functions $\phi_I(\mathbf{x})$ are zero at the nodes, which is certainly appealing from an implementation point of view. It follows from its construction that $\mathbf{u}^h(\cdot,t) \in S_t$. Note that the approximation in Equation (32) differs from the XFEM approximation for cracks [22] in that only the tangential component is discontinuous.

An approximation analogous to that in Equation (32) can be obtained for the acceleration field by differentiating the displacement approximation in (32) with respect to time:

$$\ddot{\mathbf{u}}^h(\mathbf{X},t) = \sum_{I=1}^{n_{\text{nod}}} N_I(\mathbf{X})\ddot{\mathbf{a}}_I(t) + \sum_{I\in\mathbb{J}} \phi_I(\mathbf{X}) \ddot{q}_I(t)\mathbf{e}_T(\mathbf{X}) \tag{34}$$

where $\ddot{\mathbf{a}}_I$ are the standard acceleration degrees of freedom and $\ddot{q}_I$ are the acceleration degrees of freedom associated to the enrichment. The material character of the dissipative interface Γ_{DI} has been considered for the above derivation.

Let us now define the approximation space for the displacement field as

$$S_t^h := \left\{ \mathbf{u}_t^h \in S_t;\ \ \mathbf{u}_t^h = \mathbf{u}^h(\cdot,t) \text{ in } \Omega,\ \ \mathbf{u}_t^h\Big|_{\Gamma_u} = \mathbf{u}^*(t) \right\} \tag{35}$$

where $\mathbf{u}^*(t)$ are the displacements prescribed on Γ_u at time t. Note that the approximation is conforming in the sense that $S_t^h \subset S_t$. Now the space of test functions corresponding to the finite element discretization of the IBVP stated in Equation (10) can be defined as

$$V^h := \left\{ \delta\mathbf{u}^h \in V;\ \ \delta\mathbf{u}^h = \mathbf{u}^h(\cdot,t) \text{ in } \Omega,\ \ \delta\mathbf{u}^h\Big|_{\Gamma_u} = \mathbf{0} \right\} \tag{36}$$

Copyright © 2005 John Wiley & Sons, Ltd.

After substituting the approximations for the displacements, the accelerations, and the test functions in Equation (10), the following semi-discrete weak form of the IBVP can be obtained:

$$\sum_{I=1}^{n_{\text{nod}}} (\delta \mathbf{a}_I) \cdot \left(\mathbf{f}_I^{\text{int}} + \mathbf{M}_{IK}^{a} \cdot \ddot{\mathbf{a}}_K + \mathbf{M}_{IK}^{\text{aq}} \ddot{q}_K - \mathbf{f}_I^{\text{ext}} \right) + \sum_{I \in \mathbb{J}} \delta q_I \left(Q_I^{\text{int}} + \mathbf{M}_{IK}^{q} \ddot{q}_K + \mathbf{M}_{IK}^{\text{aq}} \cdot \ddot{\mathbf{a}}_K - Q_I^{\text{ext}} \right) = 0 \tag{37}$$

for all kinematically admissible $\delta \mathbf{a}_I$ and δq_I. In the above,

$$\begin{aligned} \mathbf{f}_I^{\text{int}} &= \int_{\Omega \setminus \Gamma_{\text{DI}}} \nabla N_I \cdot \boldsymbol{\sigma} \, \mathrm{d}\Omega \\ \mathbf{f}_I^{\text{ext}} &= \int_{\Gamma_\sigma} N_I \mathbf{t} \, \mathrm{d}\Gamma + \int_{\Omega} N_I \mathbf{b} \, \mathrm{d}\Omega \end{aligned} \tag{38}$$

$$\begin{aligned} Q_I^{\text{int}} &= \int_{\Omega \setminus \Gamma_{\text{DI}}} (\nabla \phi_I \odot \mathbf{e}_T) : \boldsymbol{\sigma} \, \mathrm{d}\Omega + \int_{\Omega \setminus \Gamma_{\text{DI}}} \phi_I (\nabla \odot \mathbf{e}_T) : \boldsymbol{\sigma} \, \mathrm{d}\Omega \\ Q_I^{\text{ext}} &= \int_{\Gamma_{\mathbf{u}}} \phi_I (\mathbf{t} \cdot \mathbf{e}_T) \, \mathrm{d}\Gamma + \int_{\Omega} \phi_I (\mathbf{b} \cdot \mathbf{e}_T) \, \mathrm{d}\Omega - \int_{\Gamma_{\text{DI}}} [\![\phi_I]\!] t_T \, \mathrm{d}\Gamma \end{aligned} \tag{39}$$

$$\begin{aligned} \mathbf{M}_{IK}^{a} &= \int_{\Omega} N_I N_K \mathbf{1} \, \mathrm{d}\Omega \\ \mathbf{M}_{IK}^{\text{aq}} &= \int_{\Omega} N_I \phi_K \mathbf{e}_T \, \mathrm{d}\Omega \\ \mathbf{M}_{IK}^{q} &= \int_{\Omega} \phi_I \phi_K \, \mathrm{d}\Omega \end{aligned} \tag{40}$$

4.2. Discretization in time

Once the semi-discrete form of the IBVP is obtained, a numerical scheme has to be employed for integration in time. In the present work, the explicit central-difference method is used.

4.3. Quadrature

Since several of the integrands appearing in the expressions of the discretized governing equations are discontinuous at Γ_{DI}, standard quadrature rules are not well suited to the elements in which the discontinuities occur. As a consequence, a procedure based on that used by Moes *et al.* [22] is followed. First, a Delaunay triangulation is applied to the two parts into which

Copyright © 2005 John Wiley & Sons, Ltd.

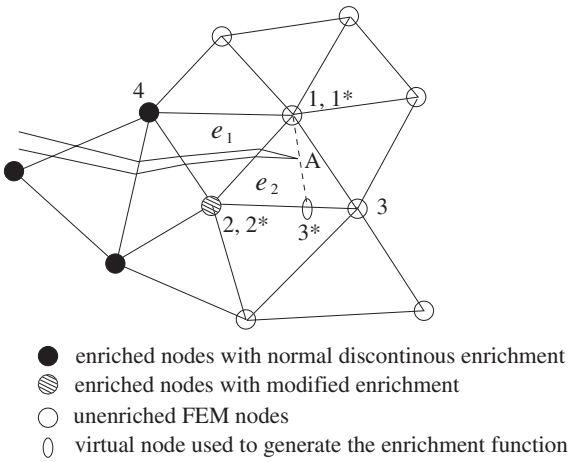


Figure 2. Schematic of the enrichment scheme for shear bands ending within an element.

the element is split by the discontinuity. Then, a standard quadrature rule is applied to each of the triangles in the tessellation.

4.4. Elements partially cut by the shear band

One of the notable features of X-FEM is its ability to model the growth of discontinuities continuously. In order to profit from this capability, the possibility of a shear band tip within an element has to be considered. In the case of elements only slit by the dissipative interface, a special procedure is used. This procedure was developed in Reference [27] and is based in the construction of a virtual triangle in such a way that it is fully cut by the shear band. Figure 2 illustrates the treatment of slit elements, for more details see Reference [27].

5. SHEAR BAND PROPAGATION

Since we are modelling shear bands as discontinuity interfaces consisting of material points for which the hyperbolicity indicator e has lost positivity, it is natural to require that its value at the tip of the shear band should fulfill the following conditions at a given time t:

$$e\left(\mathbf{x}^{\text{tip}}(t), t\right) = 0 \tag{41}$$

$$\dot{e}\left(\mathbf{x}^{\text{tip}}(t), t\right) = 0 \tag{42}$$

Note that e depends on t not only explicitly, but also through $\mathbf{x}^{\text{tip}}$. The above conditions were used in Reference [12] for crack propagation. Here, we use them to propagate the tip of the shear band. Denoting $\dot{e}^{\text{tip}} \equiv \dot{e}(\mathbf{x}^{\text{tip}}, \cdot)$, we have

$$\dot{e}^{\text{tip}} = \left(\frac{\partial e^{\text{tip}}}{\partial t}\right) + \left(\nabla e^{\text{tip}}\right) \cdot \dot{\mathbf{x}}^{\text{tip}} = 0 \tag{43}$$

Copyright © 2005 John Wiley & Sons, Ltd.

where $\dot{\mathbf{x}}^{\text{tip}}$ is the velocity of the shear band tip, which can be expressed as

$$\dot{\mathbf{x}}^{\text{tip}} = v^{\text{tip}} \mathbf{e}_T^{\text{tip}} \tag{44}$$

where v^{tip} denotes the speed of the shear band tip and $\mathbf{e}_T^{\text{tip}}$ is the unit tangent to the shear band at $\mathbf{x}^{\text{tip}}$. Then, from Equations (43) and (44), we obtain

$$v^{\text{tip}} = -\frac{1}{\nabla e^{\text{tip}} \cdot \mathbf{e}_T^{\text{tip}}} \left(\frac{\partial e^{\text{tip}}}{\partial t} \right) \tag{45}$$

If we denote the length of the dissipative interface Γ_{DI} by ℓ, then Equation (45) can be rewritten as

$$\frac{\partial \ell}{\partial t} = -\frac{1}{\nabla e^{\text{tip}} \cdot \mathbf{e}_T^{\text{tip}}} \left(\frac{\partial e^{\text{tip}}}{\partial t} \right) \tag{46}$$

The above equation can be used in the discrete IBVP to update the position of the shear band tip. The increment of ℓ at a given time step can be readily computed from (46) by using, for instance, a forward Euler time integration scheme.

6. EXAMPLES

In this section some numerical examples illustrating the performance of the methodology presented before are shown. For all the examples, the plane strain hypothesis has been adopted.

6.1. Rectangular plate subjected to pure shear

First, a rectangular plate of dimensions 1 m × 0.3 m is subjected to pure shear. This test is intended to show the performance of the enrichment when pure shear is applied. Constant velocity in the x-axis direction is applied on the lower side of the specimen. The enrichment is applied from the beginning of the computation. No cohesive force is included on the interface. Figure 3 shows the deformed mesh. Its shape does not change through time as expected.

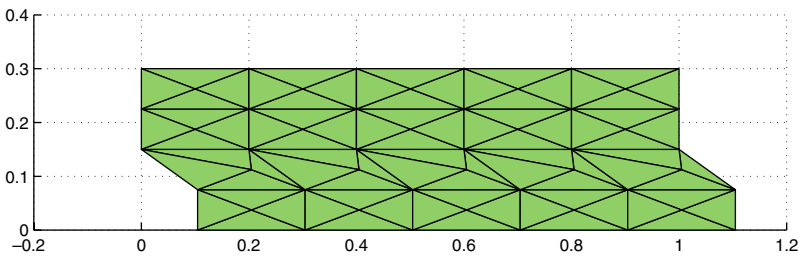


Figure 3. Rectangular plate subjected to pure shear.

Copyright © 2005 John Wiley & Sons, Ltd.

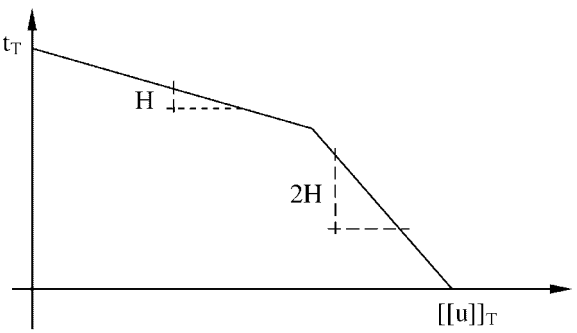


Figure 4. Traction separation law.

6.2. Rectangular plate subjected to traction

The main purpose of this example is to show the ability of the proposed methodology to predict the direction of progression of a shear band. A rectangular plate with an initial imperfection is subjected to velocity in the y-direction applied on its upper side. The velocity increases linearly until a prescribed time $t = 0.2\,\text{ns}$. Further on, it remains constant with a value of $v = 20\,\text{m/s}$. The imperfection is modelled as an initial horizontal notch.

The material parameters considered correspond to a maraging steel type 18Ni1900: Young's modulus $E = 190\,\text{GPa}$, Poisson's ratio $\nu = 0.3$, density $\rho = 8000\,\text{kg/m}^3$. An exponential softening law was employed for the continuum model. As to the traction–separation model, a bilinear law was used as shown in Figure 4.

Figure 5 shows the shear band pattern at an intermediate and at a late stage of the loading process. The dots indicate the different positions of the tip of the shear band as it evolves. The direction of propagation is approximately equal to 45° with respect to the horizontal axis during most of the interval of analysis. It is important to mention that two values of the angle of propagation are obtained from the analysis of the hyperbolicity indicator. Thus, one of them has to be selected. Since, to the knowledge of the authors, there is no generally accepted criterion to make this selection, the decision has to be made based on heuristical considerations in each case. We used a persistence criterion where the direction most closely aligned with the previous direction was chosen.

6.3. Impacted pre-notched specimen

A pre-notched specimen impacted by a flat projectile is considered. A scheme of the setup of the test is shown in Figure 6. This test is based on the experiments reported by Kalthoff and Winkler [28]. However, this simulation only aims at capturing qualitative features. Neither thermal effects nor rate dependency are considered here.

As in the preceding example, the material parameters correspond to a maraging steel type 18Ni1900: Young's modulus $E = 190\,\text{GPa}$, Poisson's ratio $\nu = 0.3$, density $\rho = 8000\,\text{kg/m}^3$. Again, an exponential softening law was employed for the continuum model and a bilinear law was used for the traction separation model.

Because of the symmetry of the problem, only the upper half of the specimen was modelled. The impactor is modelled as an initial velocity of $v = 40\,\text{m/s}$.

Copyright © 2005 John Wiley & Sons, Ltd.

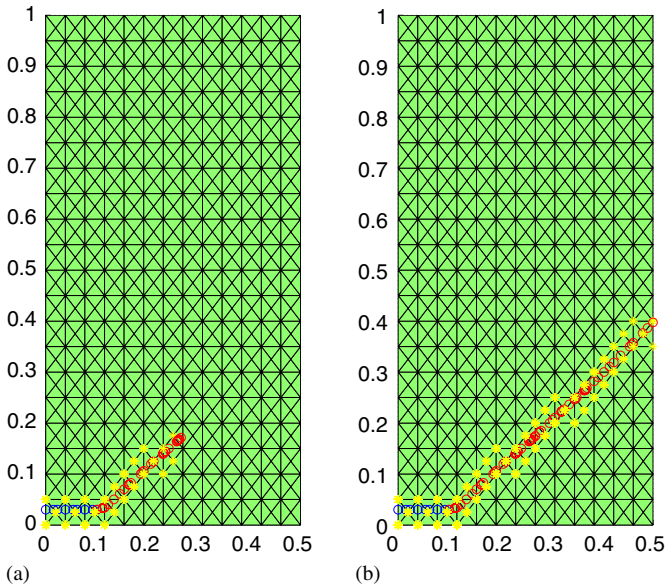


Figure 5. (a) Shear band evolution at intermediate stage; and (b) shear band evolution at late stage.

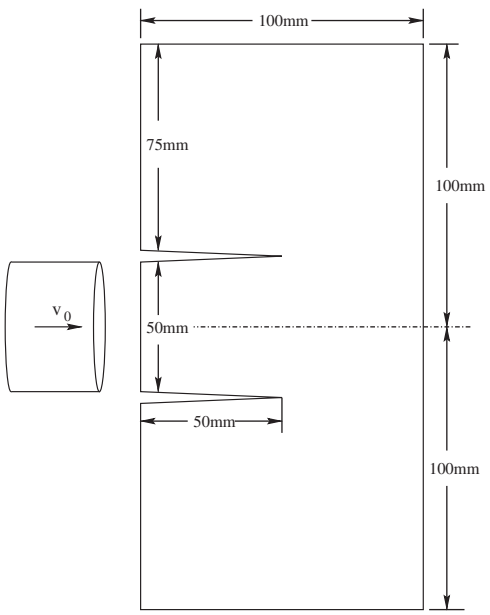


Figure 6. Impacted pre-notched specimen: experimental setup.

Two meshes with different level of refinement were used. Figure 7(a) shows the resulting shear band path for the coarser mesh. The thick solid line represents the initial notch, while the dots indicate the different points occupied by the shear band as it grows. It can be seen

Copyright © 2005 John Wiley & Sons, Ltd.

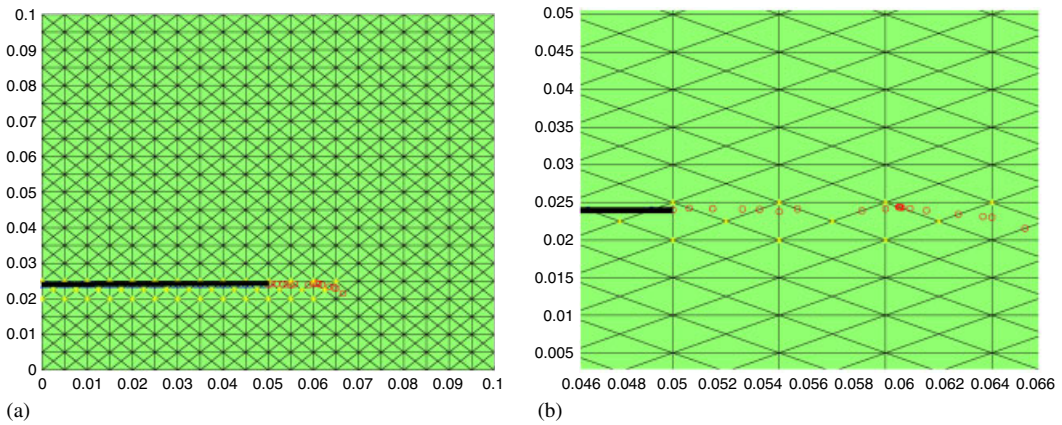


Figure 7. Impacted pre-notched specimen: (a) shear band pattern for coarser mesh; and (b) shear band pattern zoom.

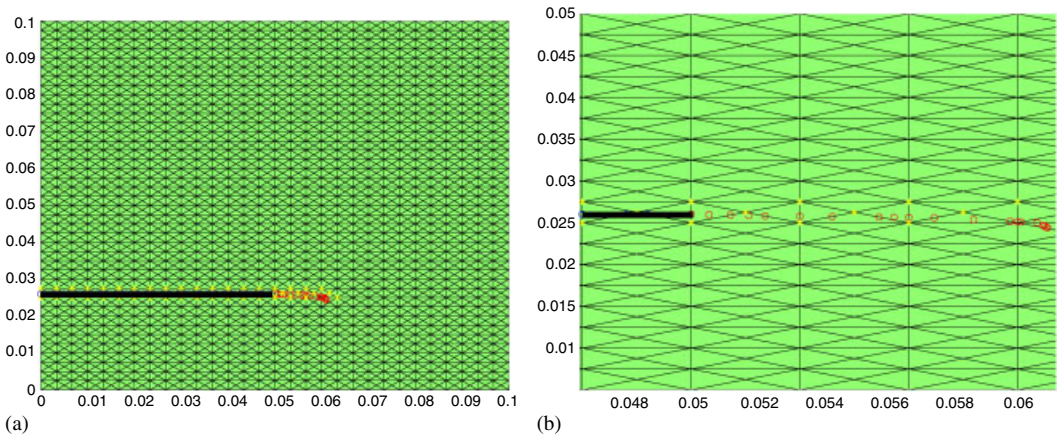


Figure 8. Impacted pre-notched specimen: (a) shear band pattern for finer mesh; and (b) shear band pattern zoom.

how the shear band penetrates into the specimen. Also, the shear band path exhibits the same downward drift as observed in experiments. Li *et al.* [29] also captured this pattern. This can be better seen in Figure 7(b), where a zoom of the region in which the shear band develops is shown.

The shear band path for the second mesh can be seen in Figure 8(a). A zoom of the region in which the shear band develops is shown in Figure 8(b). The qualitative behaviour is the same as in the coarser mesh.

Also, a plot of the shear band advance along time is shown in Figure 9. It can be seen that the progression of the shear band is intermittent. However, the average shear band tip speed of 500 m/s is reasonable.

Copyright © 2005 John Wiley & Sons, Ltd.

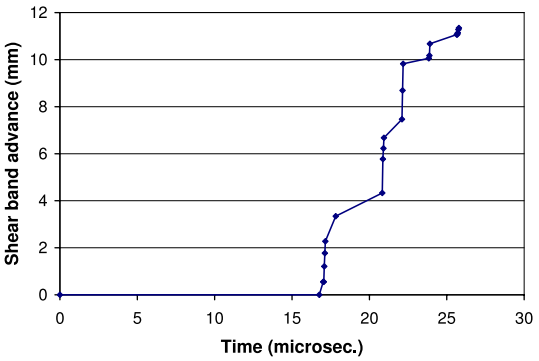


Figure 9. Shear band advance in time.

7. CONCLUDING REMARKS

A methodology to model shear bands as discontinuities in the displacement field has been presented. Its salient features are the following:

- The transition from continuum to discontinuum is governed by the loss of hyperbolicity of the (linearized) IBVP.
- The post-localization behaviour of a material point for which hyperbolicity has been lost is modelled by means of a traction–separation law.
- This traction–separation law is obtained from a continuum J2 flow plasticity model. One relevant consequence is that the normal component of the velocity jump must be equal to zero.
- The spatial discretization of the IBVP by means of X-FEM leads to a conforming approximation.
- A propagation criterion for the shear band tip can be obtained from an analysis of the value of the hyperbolicity indicator defined in Equation (2).
- The possibility of elements only partially cut by a shear band is taken into account, i.e. the shear band tip can be arbitrarily located inside an element domain.

The examples presented show that, from a qualitative point of view, the methodology presented here can be successfully applied to the study of the dynamical propagation of shear bands in solids. However, the applicability of these methods to materials where significant plastic deformation precedes the loss of hyperbolicity is not clear.

ACKNOWLEDGEMENTS

The support of the Office of Naval Research and the Army Research Office is gratefully acknowledged.

REFERENCES

1. Bazant ZP, Belytschko T. Wave propagation in a strain-softening bar: exact solution. *Journal of Engineering Mechanics* (ASCE) 1985; **111**(3):381–389.
2. Armero F. On the characterization of localized solutions in inelastic solids: an analysis of wave propagation in a softening bar. *Computer Methods in Applied Mechanics and Engineering* 2001; **191**:181–213.

Copyright © 2005 John Wiley & Sons, Ltd.

3. Ortiz M, Leroy Y, Needleman A. Finite element method for localized failure analysis. *Computer Methods in Applied Mechanics and Engineering* 1987; **61**(2):189–214.
4. Belytschko T, Fish J, Englemann B. A finite element method with embedded localization zones. *Computer Methods in Applied Mechanics and Engineering* 1988; **70**:59–89.
5. Simo JC, Oliver J, Armero F. An analysis of strong discontinuities induced by strain-softening in rate-independent inelastic solids. *Computational Mechanics* 1993; **12**:277–296.
6. Oliver J. Modelling strong discontinuities in solid mechanics via strain softening constituitive equations, Part 1: fundamentals, Part 2: numerical simulation. *International Journal for Numerical Methods in Engineering* 1996; **39**:3575–3624.
7. Armero F, Garikipati K. An analysis of strong discontinuities in multiplicative finite strain plasticity and their relation with the numerical simulation of strain localization in solids. *International Journal of Solids and Structures* 1996; **33**(20–22):2863–2885.
8. Belytschko T, Liu WK, Moran B. *Nonlinear Finite Elements for Continua and Structures*. Wiley: Chichester, 2000.
9. Marsden JE, Hughes TJR. *Mathematical Foundations of Elasticity*. Dover Publications Inc.: New York, 1983.
10. Dacorogna B. *Direct Methods in the Calculus of Variations*. Springer: Berlin, 1989.
11. Silhavy M. *The Mechanics and Thermodynamics of Continuous Media*. Springer: Berlin, 1997.
12. Belytschko T, Chen H, Xu J, Zi G. Dynamic crack propagation based on loss of hyperbolicity and a new discontinuous enrichment. *International Journal for Numerical Methods in Engineering* 2003; **58**(12): 1873–1905.
13. Dugdale D. Yielding of steel sheets containing slits. *Journal of the Mechanics and Physics of Solids* 1960; **8**:100–108.
14. Barenblatt G. The mathematical theory of equilibrium of cracks in brittle fracture. *Advances in Applied Fracture* 1962; **7**:55–129.
15. Stolarska M, Chopp DL, Moës N, Belytschko T. Modelling crack growth by level sets in the extended finite element method. *International Journal for Numerical Methods in Engineering* 2001; **51**:943–960.
16. Gravouil A, Moes N, Belytschko T. Non-planar 3d crack growth by the extended finite element and level sets—Part ii: level set update. *International Journal for Numerical Methods in Engineering* 2002; **53**: 2569–2586.
17. Ambrosio L, Coscia A, Dal Maso G. Fine properties of functions with bounded deformation. *Archives for Rational Mechanics and Analysis* 1997; **139**:201–238.
18. Simo JC, Oliver J. A new approach to the analysis and simulation of strain softening in solids. *Proceedings of the US–Europe Workshop in Fracture and Damage in Quasibrittle Structures*, 1994.
19. Oliver J. On the discrete constitutive models induced by strong discontinuity kinematics and continuum constitutive equations. *International Journal of Solids and Structures* 2000; **56**:1051–1082.
20. Olmstead WE, Nemat-Nasser S, Ni L. Shear bands as surfaces of discontinuity. *Journal of the Mechanics and Physics of Solids* 1994; **42**:697–709.
21. Oliver J, Cervera M, Manzoli O. Strong discontinuities and continuum plasticity models: the strong discontinuity approach. *International Journal of Plasticity* 1999; **15**:319–351.
22. Moes N, Dolbow J, Belytschko T. A finite element method for crack growth without remeshing. *International Journal for Numerical Methods in Engineering* 1999; **46**(1):133–150.
23. Belytschko T, Black T. Elastic crack growth in finite elements with minimal remeshing. *International Journal for Numerical Methods in Engineering* 1999; **45**(5):601–620.
24. Belytschko T, Moes N, Usui S, Parimi C. Arbitrary discontinuities in finite elements. *International Journal for Numerical Methods in Engineering* 2001; **50**(4):993–1013.
25. Wells GN, de Borst R, Sluys LJ. A consistent geometrically non-linear approach for delamination. *International Journal for Numerical Methods in Engineering* 2002; **54**:1333–1355.
26. Moes N, Belytschko T. Extended finite element method for cohesive crack growth. *Engineering Fracture Mechanics* 2002; **69**:813–834.
27. Zi G, Belytschko T. New crack-tip elements for xfem and applications to cohesive cracks. *International Journal for Numerical Methods in Engineering* 2003; **57**(15):2221–2240.
28. Kalthoff JF, Winkler S. Failure mode transition at high rates of shear loading. *International Conference on Impact Loading and Dynamic Behavior of Materials* 1987; **1**:185–195.
29. Li S, Liu WK, Rosakis AJ, Belytschko T, Hao W. Mesh free Galerkin simulations of dynamic shear band propagation and failure mode transition. *International Journal of Solids and Structures* 2002; **39**: 1213–1240.

Copyright © 2005 John Wiley & Sons, Ltd.